

# Tectonic pressure gradients during viscous creep drive fluid flow and brittle failure at the base of the seismogenic zone

Luca Menegon<sup>1</sup> and Åke Fagereng<sup>2</sup><sup>1</sup>Njord Centre, Department of Geosciences, University of Oslo, Blindern, 0316 Oslo, Norway<sup>2</sup>School of Earth and Environmental Sciences, Cardiff University, Park Place, Cardiff CF10 3AT, UK

## ABSTRACT

Fluid-pressure cycles are commonly invoked to explain alternating frictional and viscous deformation at the base of the seismogenic crust. However, the stress conditions and geological environment of fluid-pressure cycling are unclear. We address this problem by detailed structural investigation of a vein-bearing shear zone at Sagelvvatn, northern Norwegian Caledonides. In this dominantly viscous shear zone, synkinematic quartz veins locally crosscut mylonitic fabric at a high angle and are rotated and folded with the same sense of shear as the mylonite. Chlorite thermometry indicates that both veining and mylonitization occurred at ~315–400 °C. The vein-filled fractures are interpreted as episodically triggered by viscous creep in the mylonite, where quartz piezometry and brittle failure modes are consistent with low (18–44 MPa) differential stress. The Sagelvvatn shear zone is a stretching shear zone, where elevated pressure drives a hydraulic gradient that expels fluids from the shear zone to the host rocks. In low-permeability shear zones, this hydraulic gradient facilitates build-up of pore-fluid pressure until the hydrofracture criterion is reached and tensile fractures open. We propose that hydraulic gradients established by local and cyclic pressure variations during viscous creep can drive episodic fluid escape and result in brittle-viscous fault slip at the base of the seismogenic crust.

## INTRODUCTION

A long-established and fundamental aspect of the deformation of geological materials is that it generates spatial and temporal variations in tectonic pressure (Casey, 1980; Mancktelow, 2002, 2008; Schmalholz and Podladchikov, 2013). Brittle fracturing and viscous flow result in pressure gradients across rheological boundaries that are crucial for driving fluid flow during rock deformation (Mancktelow, 2008). Localized viscous shear zones, which must be weaker than the surrounding material, develop a higher pressure than the host rock when they are stretched parallel to the slip direction (i.e., “positive stretching faults”; Escher and Watterson, 1974; Means, 1989). Conversely, in brittle faults, the pressure is lower than in the adjacent rocks (Mancktelow, 2006). Thus, stretching shear zones and brittle faults are “overpressured” and “underpressured” with respect to the host rock, respectively (Mancktelow, 2008). This general principle of pres-

sure-gradient generation during deformation has been invoked to explain fluid flow at the plate scale during slab unbending (Faccenda et al., 2009, 2012; Faccenda and Mancktelow, 2010), differences in plate interface shear stress between bending and unbending slabs (Beall et al., 2021), and hydrolytic weakening in the wall rock during shear-zone widening (Oliot et al., 2014; Finch et al., 2016). We build on the concept of tectonic pressure gradients to interpret field observations of a brittle-viscous shear zone. We show that pressure gradients resulting from viscous creep in the shear zone can result in cyclic and transient hydrofracturing and fluid expulsion during ongoing creep. This creep-driven hydrofracturing may contribute to explaining the cyclic frictional-viscous deformation along single structures commonly inferred from the geological and seismological record of the fluid-rich, seismogenic subduction environment (Fagereng and Sibson, 2010; Audet and Schaeffer, 2018).

## GEOLOGICAL SETTING

The studied shear zone is situated in the Ordovician–Silurian Balsfjord Group of the Lyngen nappe, in the Uppermost Allochthon thrust sheets of the Norwegian Caledonides (Fig. 1A). The Lyngen nappe consists of ophiolites including metavolcanic and metasedimentary rocks of the Iapetus Ocean (Bergh and Andresen, 1985). In the study area, the Hølen Conglomerate of the Balsfjord Group developed east-southeast–vergent, open to tight folds during the collisional stage of the Caledonian orogeny at ~400 °C and 300–400 MPa (Bergh and Andresen, 1985) (Fig. 1B; Fig. S1 in the Supplemental Material<sup>1</sup>). The kinematics and conditions place the Balsfjord Group in the orogenic wedge at an approximate depth of 10–15 km during the Caledonian continental collision. We analyzed a 3-m-thick shear zone in the Hølen Conglomerate exposed west of Sagelvvatn. In this exposure, long, gently dipping limbs of the asymmetric folds are sheared in discrete shear zones with a top-to-the-east-southeast sense of shear (Fig. 1B). Limbs of tight folds are common locations for the development of stretching shear zones (Means, 1989).

## STRUCTURAL ANALYSIS

The shear zone developed predominantly in the folded metaconglomerate but also contains bands of chlorite-muscovite schists as much as 0.5 m thick both at its base and in the shear-zone interior (Fig. 1B). The shear zone developed an internal strain partitioning with alternating low-strain protomylonitic and high-strain mylonitic domains (Figs. 1B and 1C). The mylonitic metaconglomerate contains highly elongate quartzitic pebbles in a quartz- and carbonate-rich cement. Quartzitic pebbles lack macroscopic fractures and boudinage. Although

<sup>1</sup>Supplemental Material. Analytical methods, derivation of the failure diagram, additional field photos, photomicrographs and EBSD map, and chlorite composition data. Please visit <https://doi.org/10.1130/G49012.1> to access the supplemental material, and contact [editing@geosociety.org](mailto:editing@geosociety.org) with any questions.

CITATION: Menegon, L., and Fagereng, Å., 2021, Tectonic pressure gradients during viscous creep drive fluid flow and brittle failure at the base of the seismogenic zone: *Geology*, v. 49, p. 1255–1259, <https://doi.org/10.1130/G49012.1>

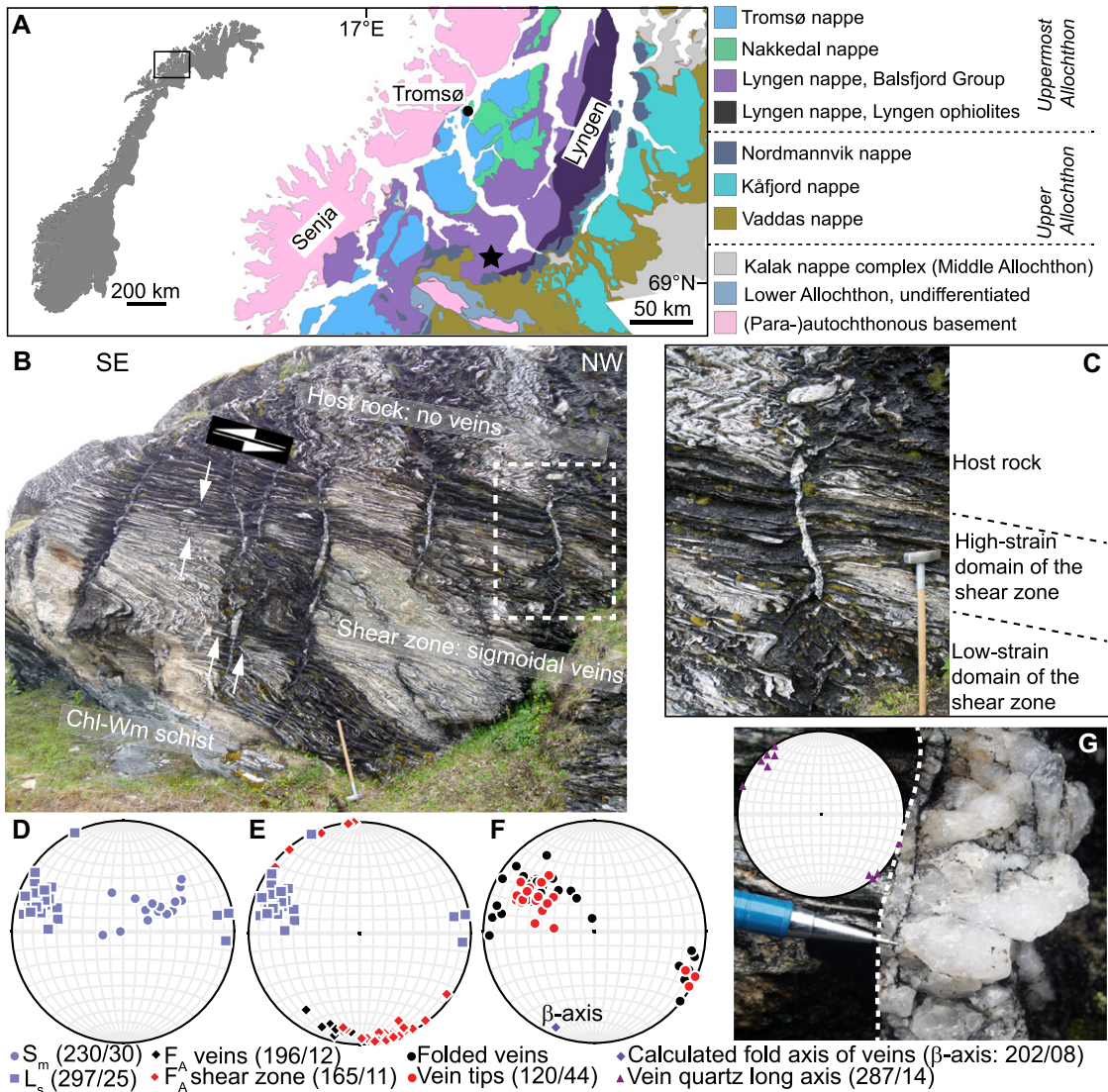


**Figure 1.** (A) Geological map of the northern Norwegian Caledonides in the Lyngen area (Norway), modified from Augland et al. (2014). Black star indicates the study area near Sagelvvatn. Location of the study area in Norway is shown in inset. (B,C) Photographs of studied outcrop (GPS coordinates, World Geodetic System 1984 datum [Universal Transverse Mercator]: 34W, 422280E, 7680841N). Dashed rectangle in B marks area of C. White arrows in B show veins that experienced large rotations with sense of shear; white arrows in the black box indicate the sense of shear. Chl-Wm—chlorite-muscovite. (D–F) Lower-hemisphere stereoplots showing orientations of: stretching lineation ( $L_s$ ) and poles to mylonitic foliation ( $S_m$ ) (D); stretching lineation and fold hinges ( $F_A$ ) of veins and folded pebbles in shear zone (E); and poles to folded veins and vein tips, and calculated hinge line of folded veins ( $\beta$ -axis) (F). Numerical values indicate average orientation of the planes or of the lines, expressed as dip direction/dip or as trend/plunge, respectively. (G) Photograph and stereoplot showing quartz vein crystal long axes orthogonal to vein wall. White dashed line indicates vein margin.

the shear zone is dominantly ductile (defined as spatially continuous deformation at the scale of observation), 1–5-cm-thick sigmoidal quartz veins, arranged *en echelon*, locally crosscut the mylonitic fabric, predominantly at a high angle (Figs. 1B and 1C). The host rock does not contain veins (Fig. 1B), although the tips of some shear zone-hosted veins extend into the host rock (Fig. 1C).

The mylonitic foliation dips gently southwest and contains a gently west-northwest–plunging stretching lineation (Fig. 1D). Lower-strain domains within the shear zone preserve decimeter-scale asymmetric, east- to east-southeast–vergent, subhorizontal parasitic folds (Figs. 1C and 1E). Higher-strain domains include SC' foliations and interconnected chlorite folia (Fig. S3C). Veins tips are oriented 50°–80° to the shear zone margins and are rotated, typically by 30°–55° relative to the vein center, with the same sense of shear as the mylonite (Fig. 1C; Fig. S2). Vein rotation occurred only inside the

high-strain zone, whereas vein tips extending into the host rocks are straight (Fig. 1C). The gently south-southwest–plunging fold hinges of the veins and the stretching lineation of the mylonite are approximately perpendicular (Figs. 1E and 1F). This indicates that the shear strain imposed on the veins was not sufficient to significantly rotate the hinge lines toward the stretching direction (Fig. 1E). Locally, however,  $\leq 75^\circ$  rotation results in a few veins being considerably thinned and lengthened in the finite stretching field (Fig. 1B; Fig. S2). Vein quartz crystals are coarse and elongate-blocky with long axes oriented 70°–80° to the vein margins and subparallel to the mylonite stretching lineation (Fig. 1G; Fig. S3).

In summary, the veins reflect the same kinematics as the mylonitic shear zone and formed and deformed during bulk viscous flow. Thus, the Sagelvvatn shear zone is an example of a relatively weak zone that is stretched parallel to its length through dominantly viscous but

locally brittle mechanisms, illustrated by subparallel mylonitic stretching lineations and vein opening vectors.

## MICROSTRUCTURES AND METAMORPHIC CONDITIONS

The matrix of the mylonitic metaconglomerate consists of large (50–200  $\mu\text{m}$ ) polygonal grains of quartz mixed with calcite, dolomite, biotite, and epidote. The mylonitic pebbles are predominantly quartzitic. Quartz grain boundaries are generally straight, and the grains are equant; however, irregular and lobate grain boundaries locally occur, indicating a component of grain-boundary migration recrystallization (Fig. 2A). Larger grains contain optically visible subgrains of 50–100  $\mu\text{m}$  (Fig. 2B). Vein quartz grains are  $\sim 200 \mu\text{m}$  to  $\sim 1.5 \text{ cm}$  long and show evidence of intracrystalline deformation in the form of arrays of blocky and elongated subgrains (Figs. S3A and S3B).

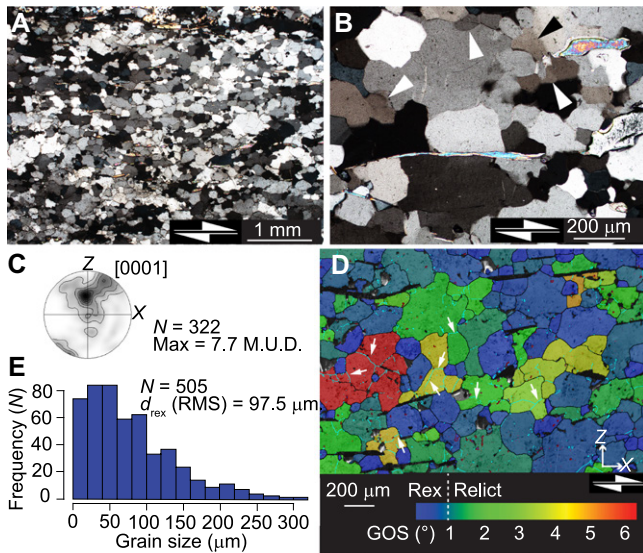


**Figure 2. (A,B) Photomicrographs of quartz microstructure in mylonitic pebbles (cross-polarized light). Arrowheads in B indicate subgrains ~100  $\mu\text{m}$  in size. White arrows in the black box indicate the sense of shear. (C–E) Results of electron backscatter diffraction analysis. (C) Crystallographic preferred orientation of quartz c-axes in mylonitic pebbles. One point per grain is plotted ( $N$  = number of grains) on lower-hemisphere projection contoured with  $15^\circ$  half-width and  $10^\circ$  cluster size. Maximum (Max) is expressed as multiples of uniform distribution (M.U.D.). Reference frame**

**is reported in D (Z—pole to mylonitic foliation; X—stretching lineation). (D) Grain orientation spread (GOS) map. Arrows indicate low-angle boundaries (in cyan) that separate subgrains ~100  $\mu\text{m}$  in size. Black lines indicate high-angle boundaries (misorientation  $>10^\circ$ ); red lines indicate Dauphiné twin boundaries. Rex—recrystallized. (E) Histogram of grain-size distribution of recrystallized quartz grains identified with GOS method.  $N$ —number of grains;  $d_{\text{rex}}$ —grain size of the recrystallized grains; RMS—root mean square.**

The temperatures of veining and mylonitic deformation were estimated with chlorite thermometry (Lanari et al., 2014) assuming a pressure of 350 MPa (Bergh and Andresen, 1985). Chlorite composition was measured from SC' fabrics indicating top-to-the-east-southeast shear in the schists and chlorite grains within the quartz veins (Fig. S3). Chlorite thermometry yields an average temperature of mylonitization of  $360 \pm 26^\circ\text{C}$  and a temperature range of 313–400  $^\circ\text{C}$  for the quartz veins (Table S1).

### MYLONITE FLOW STRESS

The quartz  $c$ -axis crystallographic preferred orientation in the mylonitic pebbles is an incomplete asymmetric crossed girdle consistent with top-to-the-east-southeast sense of shear (Fig. 2C). Low-angle boundaries are common in the larger grains and define subgrains of 50–100  $\mu\text{m}$  in size (Fig. 2D; Fig. S4). The microstructure and electron backscatter diffraction (EBSD) analyses indicate that pebble elongation was accommodated by dislocation creep in quartz, which recrystallized by subgrain rotation with a contribution of grain-boundary migration.

Following the approach of Cross et al. (2017), we used the grain orientation spread to separate recrystallized from relict grains in our samples, with a threshold of  $0.98^\circ$ . The resultant average recrystallized grain size is  $97 \pm 59 \mu\text{m}$  (root mean square  $\pm$  one standard deviation; Fig. 2E), which yields a differential stress during mylonitic flow of 18–44 MPa using the Cross et al. (2017) piezometer. Although caution is needed in applying grain-size piezometry to grains that show a contribution of grain-bound-

ary migration (Cross et al., 2017), the presence within the relict grains of subgrains with a similar size to the recrystallized grains (Figs. 2B and 2D) suggests that the grains did not grow significantly after recrystallization.

### DISCUSSION

#### Pressure Gradients Trigger Fluid Expulsion from Within the Shear Zone

The *en echelon* quartz veins are interpreted to have been triggered and controlled by viscous creep in a stretching shear zone (Fig. 1). Stretching shear zones develop a higher pressure than in the host rock, and the resulting hydraulic gradient drives expulsion of fluids from within the shear zone (Mancktelow, 2006, 2008; Finch et al., 2016). If fluids are trapped in the shear zone because of low-permeability horizons at its margins, dynamic fluid pressure may locally approach, or in thrust faulting regimes even exceed, the lithostatic pressure (Fig. 3), triggering dilatant fracturing if differential stress is low (Sibson, 1998; Cox, 2010). In the Sagelvvatn shear zone, quartz microstructure and piezometry confirm that differential stress was sufficiently low ( $<50$  MPa) for tensile fracture in frictionally strong and cohesive quartz-rich metaconglomerate (Figs. 2 and 3). Low-permeability horizons are represented by chlorite-rich schists (Fig. 1B), which typically form low-porosity seals in metamorphic environments (Ganzhorn et al., 2019). Under the same differential stress conditions as dislocation creep and tensile failure in the metaconglomerates, these frictionally weak chlorite-rich horizons likely experienced frictional sliding in interconnected chlorites (Fig. 3; Okamoto et al.,

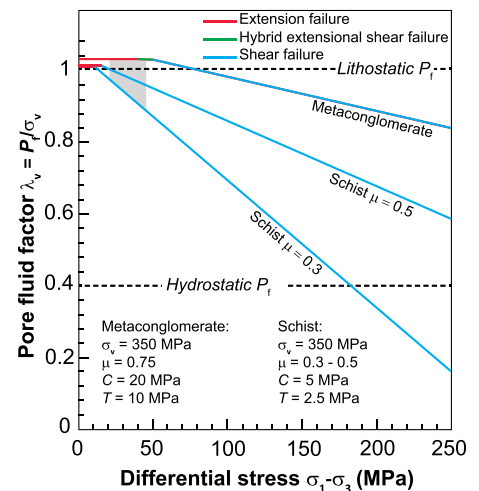


**Figure 3. Pore fluid factor ( $\lambda_v$ ) versus differential stress ( $\sigma_1 - \sigma_3$ ) failure mode diagram calculated for the Sagelvvatn shear zone (Norway), assuming optimally oriented reverse fault (see the Supplemental Material [see footnote 1] for calculations).  $P_f$ —fluid pressure;  $\sigma_v$ —vertical stress;  $\mu$ —friction coefficient;  $C$ —cohesive strength;  $T$ —tensile strength. Expected failure mode in metaconglomerate and in chlorite-rich schists at estimated flow stress in mylonite is indicated by gray area.**

2019), although direct observational evidence of this is missing in our example.

We propose a model in which tensile brittle failure occurs spontaneously within a creeping shear zone as a consequence of hydraulic gradients established by local pressure variations. In this model, the timing of fracturing is governed primarily by the rate of dynamic fluid-pressure increase during shear (Fig. 4, stage 1) until a maximum sustainable fluid overpressure is achieved and hydrofracturing occurs in frictionally strong materials (Fig. 4, stage 2). The transient fractures would be underpressured relative to the surrounding creeping matrix (Mancktelow, 2006) and represent sinks for the intergranular fluid. This decreases the pore-fluid pressure and allows creep to continue without further tensile failure (Fig. 4, stage 3) until fluid pressure builds up to trigger a new hydrofracturing episode (Fig. 4, stage 4). This process is expected to be cyclical as long as fluid pressure rises fast enough for the hydrofracture criterion to be reached before shear failure is triggered by increasing tectonic stresses. These fluid-pressure cycles originate within the creeping shear zone itself and are driven by local pressure gradients rather than external fault valving (Sibson, 1998) or local viscosity contrasts between weak matrix and strong inclusions (e.g., Hayman and Lavier, 2014; Behr et al., 2018; Beall et al., 2019).

The creep-driven hydrofracturing model might be particularly relevant to the frictional-viscous transition at the base of the seismogenic zone, where the progressive increase in the effective area of contact along a fault surface

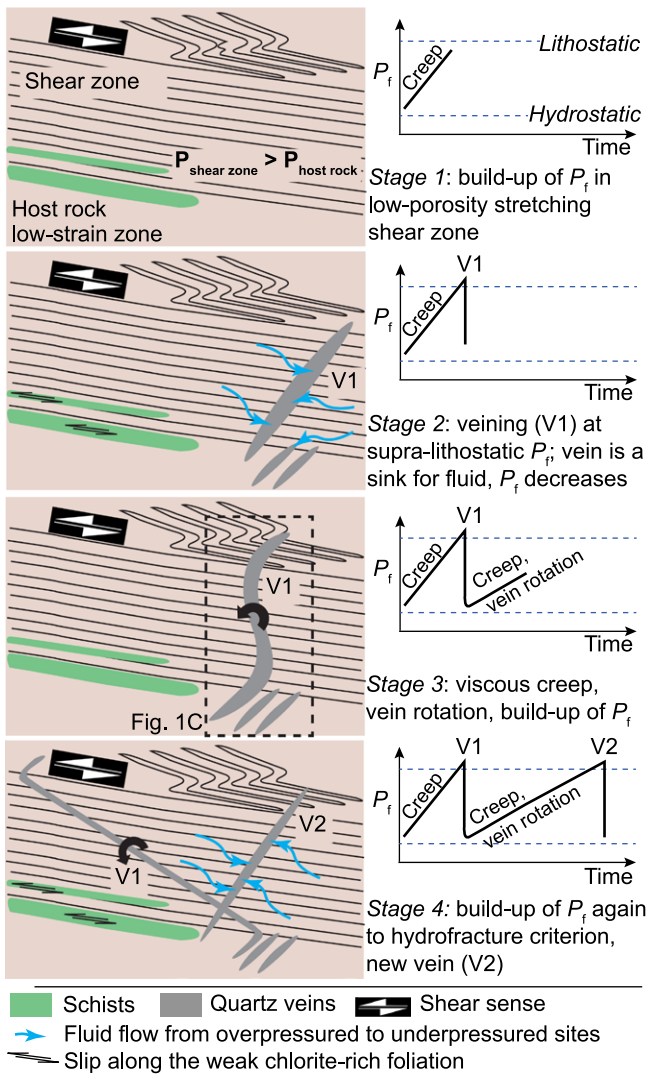


**Figure 4. Conceptual model of fluid pressure cycling and of creep-driven hydrofracturing described in the text.**  $P_{\text{shear zone}}$ —pressure in the shear zone;  $P_{\text{host rock}}$ —pressure in the host rock;  $P_f$ —fluid pressure.

ates are common, fluid release occurs from prograde dehydration, and low differential stresses prevail. These conditions fulfill all the criteria for our proposed model of creep-driven hydrofracturing, which may involve associated frictional sliding on weak, phyllosilicate-rich foliations (Figs. 3 and 4; e.g., Fagereng et al., 2018). These effects are a direct consequence of the tectonic pressure gradients that occur from outcrop to plate-boundary scale in stretching shear zones.

#### ACKNOWLEDGMENTS

This work was supported by the EU's Seventh Framework Programme (FP7) Marie Curie Career Integration Grant 618289 "EVOCOS" to L. Menegon and by the European Research Council Horizon 2020 Starting Grant 715836 "MICA" to Å Fagereng. We thank Francesca Prando for acquiring the electron microprobe analyzer data, Glenn Harper for support during scanning electron microscope work, and François Renard for discussions. Neil Mancktelow, Nick Hayman, Melanie Finch, and an anonymous reviewer provided constructive reviews that greatly improved the manuscript. Steffen Bergh and Holger Stünitz are thanked for having introduced Menegon to the study area.

#### REFERENCES CITED

- Audet, P., and Bürgmann, R., 2014, Possible control of subduction zone slow-earthquake periodicity by silica enrichment: *Nature*, v. 510, p. 389–392, <https://doi.org/10.1038/nature13391>.
- Audet, P., and Schaeffer, A.J., 2018, Fluid pressure and shear zone development over the locked to slow slip region in Cascadia: *Science Advances*, v. 4, eaar2982, <https://doi.org/10.1126/sciadv.aar2982>.
- Augland, L.E., Andresen, A., Gasser, D., and Steltenpohl, M.G., 2014, Early Ordovician to Silurian evolution of exotic terranes in the Scandinavian Caledonides of the Ofoten-Troms area—Terrane characterization and correlation based on new U-Pb zircon ages and Lu-Hf isotopic data, *in* Corfu, F., et al., eds., *New Perspectives on the Caledonides of Scandinavia and Related Areas*: Geological Society [London] Special Publication 390, p. 655–678, <https://doi.org/10.1144/SP390.19>.
- Beall, A., Fagereng, Å., and Ellis, S., 2019, Strength of strained two-phase mixtures: Application to rapid creep and stress amplification in subduction zone mélange: *Geophysical Research Letters*, v. 46, p. 169–178, <https://doi.org/10.1029/2018GL081252>.
- Beall, A., Fagereng, Å., Davies, J.H., Garel, F., and Davies, D.R., 2021, Influence of subduction zone dynamics on interface shear stress and potential relationship with seismogenic behavior: *Geochemistry Geophysics Geosystems*, v. 22, e2020GC009267, <https://doi.org/10.1029/2020GC009267>.
- Behr, W.M., Kotowski, A.J., and Ashley, K.T., 2018, Dehydration-induced rheological heterogeneity and the deep tremor source in warm subduction zones: *Geology*, v. 46, p. 475–478, <https://doi.org/10.1130/G40105.1>.
- Bergh, S.G., and Andresen, A., 1985, Tectonometamorphic evolution of the allochthonous Caledonian rocks between Malangen and Balsfjord, Troms, north Norway: *Norges Geologiske Undersøkelse Bulletin*, v. 401, p. 1–34.
- Casey, M., 1980, Mechanics of shear zones in isotropic dilatant materials: *Journal of Structural Geology*, v. 2, p. 143–147, [https://doi.org/10.1016/0191-8141\(80\)90044-9](https://doi.org/10.1016/0191-8141(80)90044-9).

facilitates the build-up of pore-fluid pressure (Hirth and Beeler, 2015). Pressure gradients resulting from viscous creep would contribute to the build-up of fluid pressure until a brittle failure criterion is reached and the overpressured fluid is driven into vein and/or fault systems.

#### Implications for Mixed Brittle-Viscous Fault-Slip Behavior

Fluid-pressure cycles are commonly invoked to explain mixed aseismic-seismic fault slip behavior at the base of the seismogenic zone, particularly in subduction zones and accretionary wedges, suggesting a link between fault-zone hydrology and fault-slip behavior (e.g., Audet and Bürgmann, 2014; Fagereng et al., 2018; Kotowski and Behr, 2019; Gosselin et al., 2020). Our observations (Figs. 1 and 2) and considerations of brittle failure modes as a function of fluid pressure and differential stress (Fig. 3) suggest that in stretching shear zones where differential stress is low and fluids are confined, fluid overpressure increasing rapidly relative to tectonic stresses leads to episodic fracture events as a direct consequence of

creep (Fig. 4). Vein-filled tensile fractures can be directly observed in the Sagelvatn shear zone. However, frictional sliding would also be triggered on frictionally weak, lower-cohesion, phyllosilicate-rich horizons at the same conditions we estimate for mylonitic shear and tensile vein opening in the metaconglomerate (Fig. 3). We cannot observationally constrain whether this frictional sliding was episodic or continuous, but it would have occurred only when a certain minimum fluid pressure was reached that allowed frictional resistance to be overcome (Fig. 3). It is therefore conceivable that hydrofracturing in the Sagelvatn shear zone also involved transient frictional shear deformation, analogous to experiments in serpentine where reaction-induced extension and shear fractures developed simultaneously (Zheng et al., 2019).

We propose that tectonically induced pressure gradients can control fluid-pressure cycling characteristic of the brittle-viscous fault-slip behavior commonly observed at the base of the seismogenic zone. This effect is likely most pronounced along the subduction thrust interface, where low-permeability phyllosili-

- Cox, S.F., 2010, The application of failure mode diagrams for exploring the roles of fluid pressure and stress states in controlling styles of fracture-controlled permeability enhancement in faults and shear zones: *Geofluids*, v. 10, p. 217–233, <https://doi.org/10.1111/j.1468-8123.2010.00281.x>.
- Cross, A.J., Prior, D.J., Stipp, M., and Kidder, S., 2017, The recrystallized grain size piezometer for quartz: An EBSD-based calibration: *Geophysical Research Letters*, v. 44, p. 6667–6674, <https://doi.org/10.1002/2017GL073836>.
- Escher, A., and Watterson, J., 1974, Stretching fabrics, folds and crustal shortening: *Tectonophysics*, v. 22, p. 223–231, [https://doi.org/10.1016/0040-1951\(74\)90083-3](https://doi.org/10.1016/0040-1951(74)90083-3).
- Faccenda, M., and Mancktelow, N.S., 2010, Fluid flow during unbending: Implications for slab hydration, intermediate-depth earthquakes and deep fluid subduction: *Tectonophysics*, v. 494, p. 149–154, <https://doi.org/10.1016/j.tecto.2010.08.002>.
- Faccenda, M., Gerya, T.V., and Burlini, L., 2009, Deep slab hydration induced by bending-related variations in tectonic pressure: *Nature Geoscience*, v. 2, p. 790–793, <https://doi.org/10.1038/ngeo656>.
- Faccenda, M., Gerya, T.V., Mancktelow, N.S., and Moresi, L., 2012, Fluid flow during slab unbending and dehydration: Implications for intermediate-depth seismicity, slab weakening and deep water recycling: *Geochemistry Geophysics Geosystems*, v. 13, p. 1–23, <https://doi.org/10.1029/2011GC003860>.
- Fagereng, Å., and Sibson, R.H., 2010, Mélange rheology and seismic style: *Geology*, v. 38, p. 751–754, <https://doi.org/10.1130/G30868.1>.
- Fagereng, Å., Diener, J.F.A., Meneghini, F., Harris, C., and Kvadsheim, A., 2018, Quartz vein formation by local dehydration embrittlement along the deep, tremorgenic subduction thrust interface: *Geology*, v. 46, p. 67–70, <https://doi.org/10.1130/G39649.1>.
- Finch, M.A., Weinberg, R.F., and Hunter, N.J.R., 2016, Water loss and the origin of thick ultramylonites: *Geology*, v. 44, p. 599–602, <https://doi.org/10.1130/G37972.1>.
- Ganzhorn, A.C., Pilorgé, H., and Reynard, B., 2019, Porosity of metamorphic rocks and fluid migration within subduction interfaces: *Earth and Planetary Science Letters*, v. 522, p. 107–117, <https://doi.org/10.1016/j.epsl.2019.06.030>.
- Gosselin, J.M., Audet, P., Estève, C., McLellan, M., Mosher, S.G., and Schaeffer, A.J., 2020, Seismic evidence for megathrust fault-valve behavior during episodic tremor and slip: *Science Advances*, v. 6, eaay5174, <https://doi.org/10.1126/sciadv.aay5174>.
- Hayman, N.W., and Lavier, L.L., 2014, The geologic record of deep episodic tremor and slip: *Geology*, v. 42, p. 195–198, <https://doi.org/10.1130/G34990.1>.
- Hirth, G., and Beeler, N.M., 2015, The role of fluid pressure on frictional behavior at the base of the seismogenic zone: *Geology*, v. 43, p. 223–226, <https://doi.org/10.1130/G36361.1>.
- Kotowski, A.J., and Behr, W.M., 2019, Length scales and types of heterogeneities along the deep subduction interface: Insights from exhumed rocks on Syros Island, Greece: *Geosphere*, v. 15, p. 1038–1065, <https://doi.org/10.1130/GES02037.1>.
- Lanari, P., Wagner, T., and Vidal, O., 2014, A thermodynamic model for di-trioctahedral chlorite from experimental and natural data in the system MgO-FeO-Al<sub>2</sub>O<sub>3</sub>-SiO<sub>2</sub>-H<sub>2</sub>O: Applications to *P-T* sections and geothermometry: *Contributions to Mineralogy and Petrology*, v. 167, 968, <https://doi.org/10.1007/s00410-014-0968-8>.
- Mancktelow, N.S., 2002, Finite-element modeling of shear zone development in viscoelastic materials and its implications for localisation of partial melting: *Journal of Structural Geology*, v. 24, p. 1045–1053, [https://doi.org/10.1016/S0191-8141\(01\)00090-6](https://doi.org/10.1016/S0191-8141(01)00090-6).
- Mancktelow, N.S., 2006, How ductile are ductile shear zones?: *Geology*, v. 34, p. 345–348, <https://doi.org/10.1130/G22260.1>.
- Mancktelow, N.S., 2008, Tectonic pressure: Theoretical concepts and modelled examples: *Lithos*, v. 103, p. 149–177, <https://doi.org/10.1016/j.lithos.2007.09.013>.
- Means, W.D., 1989, Stretching faults: *Geology*, v. 17, p. 893–896, [https://doi.org/10.1130/0091-7613\(1989\)017<0893:SF>2.3.CO;2](https://doi.org/10.1130/0091-7613(1989)017<0893:SF>2.3.CO;2).
- Oliot, E., Goncalves, P., Schulmann, K., Marquer, D., and Lexa, O., 2014, Mid-crustal shear zone formation in granitic rocks: Constraints from quantitative textural and crystallographic preferred orientations analyses: *Tectonophysics*, v. 612–613, p. 63–80, <https://doi.org/10.1016/j.tecto.2013.11.032>.
- Okamoto, A.S., Verberne, B.A., Niemeijer, A.R., Takahashi, M., Shimizu, I., Ueda, T., and Spiers, C.J., 2019, Frictional properties of simulated chlorite gouge at hydrothermal conditions: Implications for subduction megathrusts: *Journal of Geophysical Research: Solid Earth*, v. 124, p. 4545–4565, <https://doi.org/10.1029/2018JB017205>.
- Schmalholz, S.M., and Podladchikov, Y.Y., 2013, Tectonic overpressure in weak crustal-scale shear zones and implications for the exhumation of high-pressure rocks: *Geophysical Research Letters*, v. 40, p. 1984–1988, <https://doi.org/10.1002/grl.50417>.
- Sibson, R.H., 1998, Brittle failure mode plots for compressional and extensional tectonic regimes: *Journal of Structural Geology*, v. 20, p. 655–660, [https://doi.org/10.1016/S0191-8141\(98\)00116-3](https://doi.org/10.1016/S0191-8141(98)00116-3).
- Sibson, R.H., Robert, F., and Poulsen, K.H., 1988, High-angle reverse faults, fluid-pressure cycling, and mesothermal gold-quartz deposits: *Geology*, v. 16, p. 551–555, [https://doi.org/10.1130/0091-7613\(1988\)016<0551:HARFFP>2.3.CO;2](https://doi.org/10.1130/0091-7613(1988)016<0551:HARFFP>2.3.CO;2).
- Zheng, X., Cordonnier, B., McBeck, J., Boller, E., Jamtveit, B., Zhu, W., and Renard, F., 2019, Mixed-mode strain localization generated by hydration reactions at crustal conditions: *Journal of Geophysical Research: Solid Earth*, v. 124, p. 4507–4522, <https://doi.org/10.1029/2018JB017008>.

Printed in USA